Preprint typeset using LaTeX style emulateapj v. 08/13/06

THE OUTERMOST EJECTA OF TYPE Ia SUPERNOVAE

MASAOMI TANAKA[1], PAOLO A. MAZZALI[2,3,4], STEFANO BENETTI[5], KEN'ICHI NOMOTO[1,4,6], NANCY ELIAS-ROSA[2], RUBINA KOTAK[7], GIULIANO PIGNATA[8,9], VALLERY STANISHEV[10], AND STEPHAN HACHINGER[2]

Accepted for publication in The Astrophysical Journal

ABSTRACT

The properties of the highest velocity ejecta of normal Type Ia supernovae (SNe Ia) are studied via models of very early optical spectra of 6 SNe. At epochs earlier than 1 week before maximum, SNe with a rapidly evolving Si II λ6355 line velocity (HVG) have a larger photospheric velocity than SNe with a slowly evolving Si II λ6355 line velocity (LVG). Since the two groups have comparable luminosities, the temperature at the photosphere is higher in LVG SNe. This explains the different overall spectral appearance of HVG and LVG SNe. However, the variation of the Ca II and Si II absorptions at the highest velocities ($v \gtrsim 20{,}000$ km s^{-1}) suggests that additional factors, such as asphericity or different abundances in the progenitor white dwarf, affect the outermost layers. The C II λ6578 line is marginally detected in 3 LVG SNe, suggesting that LVG undergo less intense burning. The carbon mass fraction is small, only less than 0.01 near the photosphere, so that he mass of unburned C is only $\lesssim 0.01 M_{\odot}$. Radioactive ^{56}Ni and stable Fe are detected in both LVG and HVG SNe. Different Fe-group abundances in the outer layers may be one of the reasons for spectral diversity among SNe Ia at the earliest times. The diversity among SNe Ia at the earliest phases could also indicate an intrinsic dispersion in the width-luminosity relation of the light curve.

Subject headings: supernovae: general — supernovae: individual (SN 2001el, SN 2002bo, SN 2002dj, SN 2002er, SN 2003cg, SN 2003du) — radiative transfer — line: profiles

1. INTRODUCTION

Type Ia supernovae (SNe Ia) are believed to be thermonuclear explosions of CO white dwarfs (WDs). Because of their high luminosity together with a tight relation between the maximum brightness and decline rate of the light curve (LC), SNe Ia are one of the most accurate distance indicators (e.g., Phillips 1993; Riess et al. 1998; Perlmutter et al. 1999; Knop et al. 2003; Riess et al. 2004; Astier et al. 2006; Wood-Vasey et al. 2007).

In addition to the homogeneity of the LC, optical spectra of SNe Ia are also rather homogeneous. The ratio of two Si II lines in spectra at maximum correlates well with the SN luminosity (Nugent et al. 1995). The width of the Fe emission line in the nebular spectra also correlates with the LC decline rate (Mazzali et al. 1998). These works show that the spectral properties both at maximum brightness and at the nebular phases are determined primarily by the maximum luminosity.

However, recent studies using large samples revealed large diversity in the early spectra of SNe Ia, in particular in the line velocities (see e.g., Hatano et al. 2000; Benetti et al. 2005, hereafter B05; Branch et al. 2006). B05 divided SNe Ia into three groups according to the post-maximum evolution of the Si II λ6355 line velocity. High Velocity Gradient (HVG) SNe have a large Si II line velocity that decreases rapidly after maximum. On the other hand, Low Velocity Gradient (LVG) SNe have a lower velocity with a slower post-maximum evolution (see Fig. 1 in B05). HVG and LVG SNe have similar maximum luminosities, implying that line velocity is independent of luminosity or LC shape (see Fig. 3 in Hachinger, Mazzali & Benetti 2006). FAINT SNe are characterized by a lower luminosity and a low Si II line velocity, whose evolution is comparable to that of LVG SNe.

The origin of the spectral diversity is not yet fully understood, reflecting uncertainties on the explosion mechanism. Despite general consensus that burning starts as a subsonic deflagration (Nomoto, Sugimoto & Neo 1976; Nomoto, Thielemann & Yokoi 1984), it is still unclear whether or not a transition to a supersonic detonation (Khokhlov 1991b) occurs. In recent years, the explosion mechanism has been studied by detailed numerical simulations free from spherically symmetry (e.g., Reinecke, Hillebrandt, & Niemeyer 2002; Gamezo et al. 2003; Plewa, Calder & Lamb 2004; Röpke & Hillebrandt 2005; Gamezo, Khokhlov & Oran 2005).

Early phase spectra are an unique tool to investigate the state of the outer layers of the ejecta, i.e., the final fate of the burning front. Furthermore, as diversity in line velocities is largest at pre-maximum phases, modeling spectra at these epochs is likely to yield clues as to the origins of this diversity. Although several studies focussed on spectral diversity at maximum light (e.g. Bongard et al. 2006; Branch et al. 2006; Hachinger et al. 2006), only few have addressed pre-maximum spectra (e.g. Mazzali et al. 1993, Fisher et al. 1997; Mazzali 2001; Branch et al. 2007). This is mostly due to the lack of very early data, which stems from the difficulty in discovering SNe well before maximum. In order to remedy this

[1] Department of Astronomy, Graduate School of Science, University of Tokyo, Hongo 7-3-1, Bunkyo-ku, Tokyo 113-0003, Japan; mtanaka@astron.s.u-tokyo.ac.jp

[2] Max-Planck-Institut für Astrophysik, Karl-Schwarzschild-Str. 1, D-85741 Garching bei München, Germany

[3] Istituto Nazionale di Astrofisica - Osservatorio Astronomico di Triste, Via Tiepolo 11, I-34131 Triste, Italy

[4] Research Center for the Early universe, School of Science, University of Tokyo, Bunkyo-ku, Tokyo 113-0033, Japan

[5] Istituto Nazionale di Astrofisica - Osservatorio Astronomico di Padova, vicolo dell'Osservatorio 5 - 35122 Padova, Italy

[6] Institute for the Physics and Mathematics of the Universe, University of Tokyo, Kashiwa, Chiba 277-8582, Japan

[7] Astrophysics Research Centre, School of Mathematics and Physics, Queen's University Belfast, BT7 1NN, UK

[8] Departamento de Astronomía y Astrofísica, Pontificia Universidad Católica de Chile, Casilla 306, Santiago 22, Chile

[9] Departamento de Astronomía, Universidad de Chile, Casilla 36-D, Santiago, Chile

[10] Department of Physics, Stockholm University, AlbaNova University Center, SE-10691 Stockholm, Sweden

situation, the European Supernova Collaboration (ESC [11]) has endeavored to gather very early spectra of nearby SNe Ia.

One of the most interesting results of very early SN Ia spectroscopy is the possible presence of unburned carbon in the outer layers. This may be a critical signature of the outer extent of burning. The C II λ6578 line has been detected in SN 1998aq (at $\sim$ 11,000 km s^{-1}, Branch et al. 2003) and in SN 1999ac (at $\sim$ 16,000 km s^{-1}, Garavini et al. 2005). The clearest C II features were seen in a pre-maximum spectrum of SN 2006D (at $\sim$ 12,000 km s^{-1}, Thomas et al. 2006) [12]. On the other hand, C I in near-infrared (NIR) spectra has never been firmly detected (Marion et al. 2006).

High-velocity absorption features (HVFs, $v \gtrsim 20,000$ km s^{-1}) in the Ca II IR triplet (e.g., Hatano et al. 1999; Mazzali et al. 2005a; Thomas et al. 2004; Quimby et al. 2006) may be a feature of all SNe Ia at the earliest epochs (Mazzali et al. 2005b), and may indicate aspherical ejecta, as suggested by the high polarization level (Wang et al. 2003; Kasen et al. 2003). They may result from the explosion itself (Thomas et al. 2004; Mattila et al. 2005) or from the interaction of the ejecta with circumstellar medium (CSM; Gerardy et al. 2004; Mazzali et al. 2005a). The variation and distribution of the strength of Ca II HVFs may be explained by line-of-sight effects if HVFs result from aspherical structures like a few blobs or a thick disk at $v \sim 18-25,000$ km s^{-1} (Tanaka et al. 2006).

In this paper, we use SNe Ia pre-maximum optical spectra to study the physical properties of the ejecta, modeling the spectra using a numerical code. Details of the method are presented in §2. The results of the modeling are shown in §3. In §4, our results are summarized and the implications are discussed. Finally, conclusions are in §5.

2. METHOD OF ANALYSIS

Spectra of 6 nearby SNe Ia observed earlier than 1 week before maximum are studied (Table 1). The data were obtained by the ESC campaign. The ESC has collected photometric and spectroscopic data of a number of nearby SNe Ia with very good temporal and wavelength coverage. SNe with very early spectra include SN 2001el (LVG; Mattila et al. 2005), SN 2002bo (HVG; Benetti et al. 2004), SN 2002dj (HVG; Pignata et al. 2005), SN 2002er (HVG; Pignata et al. 2004; Kotak et al. 2004), SN 2003cg (LVG; Elias-Rosa et al. 2006), and SN 2003du (LVG; Stanishev et al. 2007). Our sample does not include FAINT SNe.

To investigate the physical conditions of the ejecta, such as temperatures, ionization profiles, and element abundance distribution, we use a Monte Carlo spectrum synthesis code (Mazzali & Lucy 1993), which was used for several SNe (e.g., Mazzali et al. 1993). The code requires as input the bolometric luminosity (L), photospheric velocity ($v_{\rm ph}$), and a model of the density and abundance distribution in the SN ejecta.

The code assumes a sharply defined spherical photosphere. The position of the photosphere is expressed in terms of a velocity thanks to the homologous expansion ($v \propto r$). The temperature structure of the optically thin atmosphere is solved in radiative equilibrium tracing a large number of energy packets as they propagate in the SN ejecta.

Starting from a trial temperature distribution (radiation temperature, T_R), the population of the excited level (n_j; $j = 1$ for the ground state) is computed as

$$\frac{n_j}{n_1} = W \frac{g_j}{g_1} e^{-\epsilon_j / k_B T_R}, \tag{1}$$

where g_j and ϵ_j are the statistical weight and the excitation energy from the ground level, respectively. Here W is the so called dilution factor, which is defined as

$$J = W B(T_R). \tag{2}$$

In Eq(1), W is set to unity for metastable levels (Lucy 1999). The ionization regime is computed using a modified nebular approximation (Abbott & Lucy 1985, Mazzali & Lucy 1993):

$$\frac{N_{i+1} N_e}{N_i} = \eta W \left(\frac{T_e}{T_R} \right) \left(\frac{N_{i+1} N_e}{N_i} \right)^*_{T_R}, \tag{3}$$

where N_e is the electron density and T_e the electron temperature. The starred term on the right hand side is the value computed using the Saha equation with the temperature T_R; the partition functions entering the Saha equation are, however, computed with Eq. (1). In Eq(3), η is defined as

$$\eta = \delta\zeta + W(1-\zeta), \tag{4}$$

where ζ is the fraction of recombinations going directly to the ground state. Mazzali & Lucy (1993) introduced a correction factor δ for an optically thick continuum at shorter wavelengths than the Ca II ionization edge (for a detailed definition, see Eqs. (15) and (20) in Mazzali & Lucy 1993). The second term in Eq(4) represents ionization from excited levels (Mazzali & Lucy 1993).

The Monte Carlo radiation packets are followed through the atmosphere, where they can undergo electron scattering or interact with spectral lines. For line scattering, Sobolev approximation, which is a sound approximation in a rapidly expanding medium, is applied. From the level populations, a Sobolev line opacity is obtained:

$$\tau_{lu} = \frac{hct}{4\pi}(B_{lu} n_l - B_{ul} n_u). \tag{5}$$

Here t is the time since the explosion and B_{lu} and B_{ul} are Einstein B-coefficients. The effect of photon branching is considered (Lucy 1999; Mazzali 2000; see also Pinto & Eastman 2000).

The Monte Carlo experiment gives a flux in each radial point, and then a frequency moment

$$\bar{\nu} = \frac{\int \nu J_\nu d\nu}{\int J_\nu d\nu} \tag{6}$$

is computed. Hence the temperature structure can be determined via

$$\bar{x} = \frac{h\bar{\nu}}{k_B T_R}. \tag{7}$$

Here $\bar{x}$ represents for mean energy of blackbody radiation ($\bar{x}$ = 3.832). The electron temperature is crudely assumed to be $T_e = 0.9 T_R$ to simulate approximately[13] the situation where the electron temperature is largely controlled by radiation (Klein & Castor 1978; Abbott & Lucy 1985). Level populations, ionizations and opacities are then updated using the temperature structure derived from the Monte Carlo simulation. This process is iterated until convergence.

[11] http://www.mpa-garching.mpg.de/~rtn/

[12] In SN 2006gz, the C II line is clearly seen at $\sim$ 15,000 km s^{-1}, although the SN is not normal and possibly has a super-Chandrasekhar mass progenitor (Hicken et al. 2007), as suggested for SN 2003fg (Howell et al. 2006)

[13] This assumption does not affect the spectral fitting, and thus the results in this paper, as ionization is determined mostly by the exponential part in Eq. (3) computed with T_R, which is a direct result of the Monte Carlo simulation.

TABLE 1
PROPERTIES OF THE SNE AND THE SPECTRA

Name (group)	Epoch [a]	Δm_{15} [b]	$E(B-V)$ [c]	μ [d]	$v_{\rm Si}$ [e]	$v_{\rm Ca,ph}$ [f]	$v_{\rm Ca,hv}$ [g]	References
SN 2002bo (HVG [h])	–8.0	1.17	0.38	31.67	15.0	14.9	22.1	1
SN 2002dj (HVG)	–11.0	1.12	0.10	32.98	16.8	17.7	27.6	2
SN 2002er (HVG)	–7.4	1.33	0.36	32.90	13.0	15.6	23.1	3, 4
SN 2001el (LVG [i])	–9.0	1.15	0.22	31.26	14.0	17.1	23.8	5
SN 2003cg (LVG)	–7.6	1.25	1.36	31.28	12.0	12.7	22.0	6
SN 2003du (LVG)	–11.0	1.02	0.01	32.79	12.0	15.5	22.5	7

REFERENCES. — (1) Benetti et al. (2004); (2) Pignata et al. 2005; (3) Pignata et al. (2004); (4) Kotak et al. (2005); (5) Mattila et al. (2005); (6) Elias-Rosa et al. (2006); (7) Stanishev et al. (2007)

[a]Days since B maximum
[b]Difference of B magnitude between maximum and 15 days later
[c]Color excess [sum of that caused by our Galaxy and the SN host galaxy; $R_V = 3.1$ is adopted except for the host galaxy of SN 2003cg ($R_V = 1.8, E(B-V) = 1.33$; Elias-Rosa et al. 2006)]
[d]Distance modulus (see literature)
[e]Doppler velocity of Si II λ6355 absorption minimum (10^3 km s^{-1})
[f]Doppler velocity of the photospheric component of Ca IR triplet (10^3 km s^{-1}). see Mazzali et al. (2005b)
[g]Doppler velocity of the high-velocity component of Ca IR triplet (10^3 km s^{-1}). see Mazzali et al. (2005b)
[h]High Velocity Gradient (a group of SNe Ia whose Si line velocity declines rapidly (see §1; B05), shown in blue throughout the paper)
[i]Low Velocity Gradient (a group of SNe Ia whose Si line velocity declines slowly (see §1; B05), shown in green throughout the paper)

We use the W7 deflagration model (Nomoto et al. 1984) as a standard density profile. Alternatively, a density structure of a delayed detonation model is used (model WDD2 in Iwamoto et al. 1999, hereafter, DD model). The density structures of these models are most different in layers above $v = 20,000$ km s^{-1}. The density in the DD model at $v \sim 25,000$ km s^{-1} is higher than that of W7 by a factor of ~ 10 (see Fig. 11 in Baron et al. 2006). Thus the "density enhancement" referred to in Mazzali et al. (2005a) is equivalent to the structure of the DD model if the densities are increased by a factor of $\lesssim 10$. The kinetic energy of the DD model (1.4×10^{51} ergs) is slightly larger than that of W7 (1.3×10^{51} ergs).

Element abundance distributions (i.e., mass fractions of elements) are parameterized for better reproduction of the observed spectra. Initially, a homogeneous abundance distribution is assumed, averaging the abundance distribution of W7 above the photospheric velocity, and a general fit of the spectrum is obtained adjusting the abundances. In this process, the input parameters L and $v_{\rm ph}$ are also optimized. Then a stratified abundance distribution is adopted and optimized to reproduce the details. In this paper, we employ two different-abundance zones except for SN 2003cg (3 zones are used; see §3.5.3).

The abundances in the outermost ejecta are further checked against the spectra at maximum. Although the photosphere recedes with time as the ejecta expand, the abundances at high velocities can still affect the synthetic spectra at later epochs (Stehle et al. 2005). Therefore we modelled the spectra at maximum using the abundance ratios derived from the pre-maximum spectra for the region at $v > v_{\rm ph}$(early), where $v_{\rm ph}$(early) is the photospheric velocity of the pre-maximum spectra. If the result is inconsistent (e.g., incorrect high-velocity absorptions resulting from the pre-maximum spectra photospheric component), the pre-maximum spectra are re-investigated until consistence is achieved.

3. RESULTS

In this section, we present the results of the modeling for each SN. The properties of the SNe and the spectra are summarized in Table 1. In addition to the parameters L and $v_{\rm ph}$, and the abundances in the ejecta, the distance modulus (μ) and the reddening [in terms of $E(B-V)$ and R_V] are also required to reproduce the observed spectra. Thus the luminosity and the epoch, which are often neglected by rescaling the flux arbitrarily, are important because $v_{\rm ph}$ is constrained not only by the line velocities but also by the relation $L \propto v_{\rm ph}^2 t^2 T_{eff}^4$. Here t is the time since the explosion and T_{eff} the effective temperature.

TABLE 2
PARAMETERS OF THE SYNTHETIC SPECTRA

Name (group)	Epoch	log(L) [a]	$v_{\rm ph}$ [b]	$T_{\rm ph}$ [c]
SN 2002bo (HVG)	–8.0	42.78	12,900	10,900
SN 2002dj (HVG)	–11.0	42.44	14,000	10,200
SN 2002er (HVG)	–7.4	42.98	9,500	17,300
SN 2001el (LVG)	–9.0	42.87	10,500	17,100
SN 2003cg (LVG)	–7.6	42.84	9,000	17,000
SN 2003du (LVG)	–11.0	42.71	10,000	18,600

[a]Bolometric luminosity (erg s^{-1}) in log
[b]Photospheric velocity (km s^{-1})
[c]Photospheric temperature (K) computed by the code taking the back-scattering effect into account

All spectra have been calibrated against the photometry. The epoch is estimated assuming a rise time of 19 days for all objects for simplicity. We take μ and $E(B-V)$ from the literature (see Table 1). Using all the quantities above, the photospheric temperature $T_{\rm ph}$ is computed in the code considering the back-scattering effect, and thus tends to be higher than T_{eff} (Mazzali & Lucy 1993; Mazzali 2000).

In order to facilitate the comparison of intrinsic colors, all spectra are displayed after correcting for reddening. The values of L and $v_{\rm ph}$ derived from modeling are shown in Table 2 along with the computed photospheric temperature ($T_{\rm ph}$), while the abundances of the elements at the photosphere that most affect the synthetic spectra are shown in Table 3. The abundances in the outer shell are not strongly constrained because of the lack of strong lines. Only Ca II has high velocity lines (see following sections), and the Ca mass fraction in the outer shell is shown in the table ($X_{\rm HV}$(Ca)). The iron mass fraction X(Fe) indicates the sum of stable Fe and ^{56}Fe pro-

TABLE 3
MASS FRACTIONS USED FOR THE SYNTHETIC SPECTRA

Name (group)	Epoch	X(C)[a]	X(Si)[b]	X(S)[c]	X(Ca)[d]	$X_{\rm HV}^{\rm W7}$(Ca)[e]	$X_{\rm HV}^{\rm DD}$(Ca)[f]	X(Fe)$_0$[g]	X(^{56}Ni)$_0$[h]
SN 2002bo (HVG)	–8.0	—	0.51	0.10	0.02	0.20/0.02	0.02/0.006	0.020	0.045
SN 2002dj (HVG)	–11.0	—	0.50	0.09	0.02	>0.80/0.08	0.02/0.005	0.005	0.0052
SN 2002er (HVG)	–7.4	—	0.76	0.12	0.05	0.40/0.05	0.05/0.007	0.012-0.013	< 0.025
SN 2001el (LVG)	–9.0	0.003	0.42	0.05	0.02	> 0.80/0.10	0.10/0.02	0.048	0.19
SN 2003cg (LVG)	–7.6	< 0.002	0.40 (0.08[i])	0.080	0.02	0.03/0.005	0.001/0.0001	0.0033-0.0036	< 0.0088
SN 2003du (LVG)	–11.0	0.002	0.29	0.060	0.016	0.70/0.11	0.10/0.015	0.003	0.005

[a]Mass fraction of C at the photosphere
[b]Mass fraction of Si at the photosphere
[c]Mass fraction of S at the photosphere
[d]Mass fraction of Ca at the photosphere
[e]Mass fraction of Ca in the high-velocity layers with the density structure of W7 model without/with CSM interaction
[f]Mass fraction of Ca in the high-velocity layers with the density structure of the DD model without/with CSM interaction
[g]Mass fraction of *stable* Fe (Fe except for ^{56}Fe from ^{56}Co decay) at the photosphere
[h]Mass fraction of ^{56}Ni at the photosphere (at the time of the explosion)
[i]Mass fraction of Si in the intermediate shell at $v = 17,000-20,500$ km s^{-1}

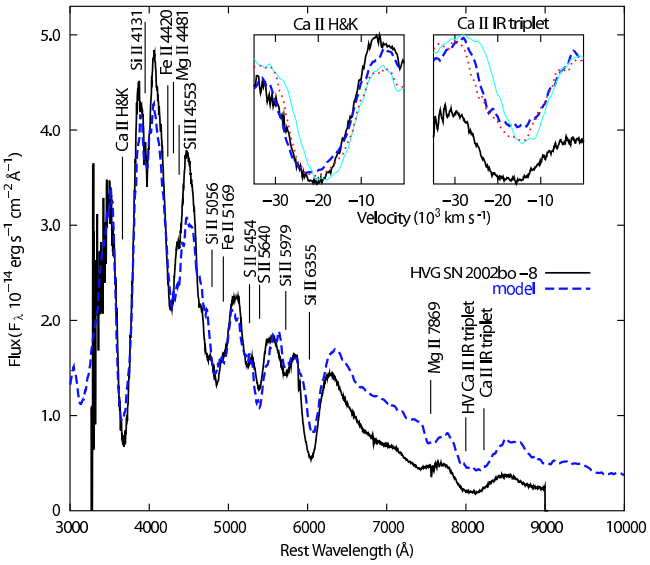

FIG. 1.— Observed spectrum of the HVG SN 2002bo at day –8 (black solid) and a model with W7-CSM density/abundance structure (blue dashed). The left inset shows the Ca II H&K feature (mean $\lambda \sim 3950$), the right inset the Ca II IR feature (mean $\lambda \sim 8567$). The W7-CSM spectrum is compared to W7/homogeneous abundance (thin cyan) and DD (dotted red) models, both without CSM interaction. In both insets, the wavelength scale is replaced by the corresponding Doppler velocies.

duced by ^{56}Ni decay at the time of the observation. If only stable Fe is considered, this is explicitely denoted as X(Fe)$_0$, where the index "0" means "at explosion". Furthermore, we use X(^{56}Ni)$_0$ for the initial mass fraction of ^{56}Ni at the time of the explosion.

3.1. *SN 2002bo (Day –8, HVG)*

3.1.1. *General Properties*

The well-studied SN 2002bo (Stehle et al. 2005) is a member of the HVG group. The spectrum at –8 days is shown in Figure 1, together with our synthetic spectrum. Good agreement is obtained with $\log L$ (erg s^{-1}) = 42.78 and $v_{\rm ph}$ = 12,900 km s^{-1}, giving a $T_{\rm ph}$ = 10,900 K. The flux redward of $\lambda \sim 6000$ Å is overestimated (see also Stehle et al. 2005). This may be due to a deviation from the blackbody approximation. A modified input radiation field, where the blue region ($\lambda \lesssim 5000$ Å) has greater weight, can reproduce the spectrum better, with only a small difference in the photospheric temperature and ionization states compared to the original case.

3.1.2. *Iron-group Elements*

An absorption feature around 4300 Å results mainly from Mg II λ4481 and Fe III λ4420, with a smaller contribution by Si III λ4553. Around 4800 Å, many Fe II and Si II lines, e.g., Fe II λ5169 and Si II λ5056, produce the strong absorption feature. To account for these strong features, the mass fraction of Fe, including both stable Fe and decay products of ^{56}Ni, should be X(Fe)=0.022 at the photosphere.

Our method of estimating the Fe abundance is illustrated in Figure 2, right panel. For solar Fe abundance, the absorption at 4950 Å (mainly Fe II λ5169) is weaker than the observed feature (red solid line). On the other hand, Fe-rich ejecta [X(Fe)$\gtrsim$0.10] produce too strong a feature (dotted line).

The abundance of radioactive ^{56}Ni synthesized in the explosion can be estimated using the Ni and Co lines that are present around 2000-4000Å. Since at $t \sim 10$ days around 30% of ^{56}Ni has not yet decayed, the strong Ni II λ4067 line is useful to constrain the mass fraction. The procedure is illustrated in Figure 2, left panel. For a larger ^{56}Ni mass fraction [X(^{56}Ni)$_0$ = 0.45], the absorption at 3900 Å appears (red dotted line), which is inconsistent with the observed feature. On the other hand, when only a solar abundance of ^{56}Ni is assumed, the flux level at $\lambda < 3500$ Å becomes too high (red solid line). This is because of insufficient blocking of (near) UV photons by iron group lines. [Our code treats the blocking by iron group elements correctly, considering photon branching (Lucy 1999; Mazzali 2000)].

A ^{56}Ni mass fraction X(^{56}Ni)$_0$ = 0.045 is derived. Although the observed flux level at $\lambda < 3500$ Å is often uncertain, the upper limit of X(^{56}Ni)$_0$ is strict because it is derived from the absence of Ni II λ4067. Therefore, most Fe detected above the photosphere must be stable [X(Fe)$_0$= 0.020].

3.1.3. *Silicon and Carbon*

The ratio of the two Si II absorptions at 5800Å and 6000Å is reproduced well. A strong Si II λ6355 suggests that the photosphere resides in the Si-rich layer. The mass fraction of Si is estimated as X(Si)$\sim$0.50. The emission peak of Si II λ6355 is well developed, and there is no evidence of C II λ6578. The

blue wing of the synthetic Si II absorption is weak, suggesting that the line may be contaminated by a HVF, as are the Ca II lines (see §3.1.4). At 7500 Å, a weak absorption is seen, which is often attributed to O I λ7774. However, in the synthetic spectrum the feature is mainly due to Mg II λ7869 and Si II λ7849. These lines are actually stronger than the O I line if Mg II λ4481 and Si II λ6355 are reproduced.

3.1.4. *Calcium*

The spectrum around Ca II H&K and the Ca II IR triplet is enlarged in the insets of Figure 1. The thin cyan line shows a synthetic spectrum computed with the original W7 density structure and homogeneous abundances, setting X(Ca)=0.02. While the observed features have a blue wing extending to $v \sim 30,000$ km s^{-1} (Ca II H&K) and 27,000 km s^{-1} (Ca II IR triplet), the wing of the synthetic absorption disappears at $v \sim 27,000$ km s^{-1} and $v \sim 23,000$ km s^{-1}, respectively. This difficulty has been reported in many papers, e.g., Hatano et al. (1999) for SN 1994D, Gerardy et al. (2004) for SN 2003du, Mazzali et al. (2005a) for SN 1999ee and Mazzali et al. (2005b) for the objects in this paper. To reproduce these features [14], we test several cases.

First, we modified the abundance distribution, keeping the W7 density structure. Although the features can be reproduced with X(Ca) $\gtrsim 0.20$ at $v > 22,000$ km s^{-1}, such a large fraction is very unlikely because the Ca mass fraction in the most Ca-rich layer is $\lesssim 0.1$ in all explosion models (see e.g., Iwamoto et al. 1999). Secondly, when we use the DD density structure, the observed profile can be reproduced with X(Ca)=0.02 at $v > 22,000$ km s^{-1} (insets of Fig. 1, dotted red lines) because of the higher density at $v > 20,000$ km s^{-1}.

Finally, we test the interesting possibility that interaction with CSM leads to some abundance mixing (Gerardy et al. 2004). As discussed by Mazzali et al. (2005a), when a hydrogen-rich CSM is mixed with the ejecta, the electron density increases, favouring recombination. Therefore some fraction of Ca III, which is the dominant state (see §4.1), becomes Ca II, making the Ca II line stronger. Here we assume that the interaction causes a density jump by a factor of 4 at $v > 22,000$ km s^{-1}, corresponding to $0.01 M_\odot$ of material. Hydrogen is assumed to be mixed into the shocked region and we find that Hα does not appear as long as X(H) < 0.30 (M(H)$\sim 5 \times 10^{-3} M_\odot$) With this model, the mass fraction of Ca in the high-velocity layers is reduced to X(Ca)=0.02 (with the W7 density structure; dashed blue line in insets of Fig. 1) and X(Ca)=0.006 (with the DD density structure), respectively. The deceleration following the interaction is not considered in our computation and a more realistic hydrodynamic calculation is needed to confirm this scenario.

3.2. *SN 2002dj (Day −11, HVG)*

3.2.1. *General Properties*

SN 2002dj has a spectral sequence and LC similar to SN 2002bo (Pignata et al. 2005), and is also an HVG SN. The spectrum 11 days before B maximum is well reproduced by a synthetic spectrum with log$L$ (erg s^{-1}) = 42.44 and $v_{\rm ph}$ = 14,000 km s^{-1} (Fig. 3). Almost all lines are the same as in the spectrum of SN 2002bo, although the velocities are higher because the epoch is earlier. The photospheric temperature, 10,200 K, is also similar.

[14] Here the width of the feature and the strength of the absorption relative to the continuum are compared because of the poor fit of the continuum level.

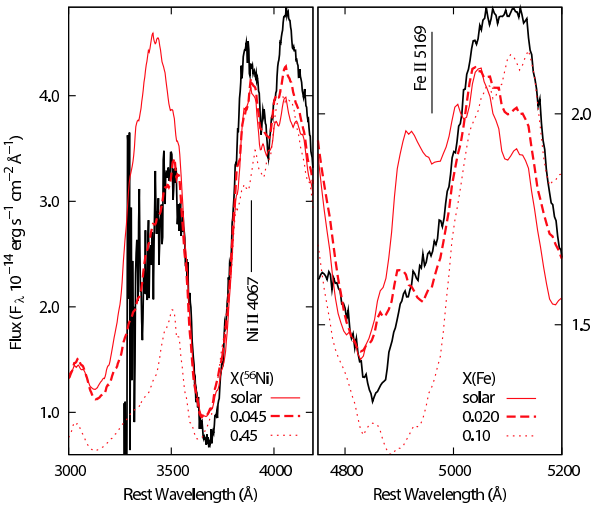

FIG. 2.— SN 2002bo: Observed spectrum around 3500 Å (*left*) and 4900 Å (*right*) compared with synthetic profiles for different metal abundances.

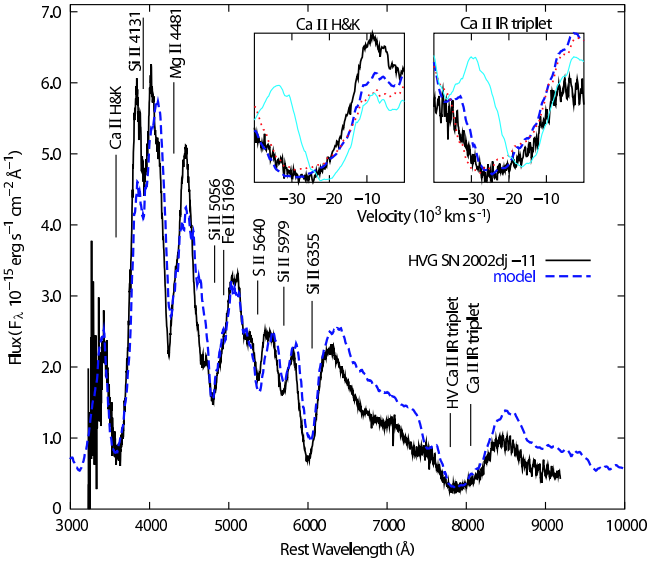

FIG. 3.— Observed spectrum of the HVG SN 2002dj at day −11 (black solid) and a model with W7-CSM density/abundance structure (blue dashed). As in Fig. 1, the insets show Ca II H&K (left) and Ca II IR (right). The W7-CSM spectrum is compared to W7 (thin cyan) and DD (dotted red) models, both with homogeneous abundance and without CSM interaction.

3.2.2. *Iron-group Elements*

Fe II and Fe III lines contribute to the features near 4200 and 4800 Å, as in SN 2002bo, but they are weaker. In fact, the absorption at 4200 Å is caused mostly by Mg II λ4481. Utilizing the feature around 4800 Å (a combination of Si II and Fe II lines) as in §3.1.2, the mass fraction of Fe is evaluated as X(Fe) ~ 0.005 at the photosphere. The features at 3500 and 3900Å require $X(^{56}\mathrm{Ni})_0 = 0.005$. Therefore, the Fe causing the observed spectral features is again mostly stable Fe. Although the values are smaller than those of SN 2002bo, they are still larger than the solar abundances by a factor of 3.5 and 70 for Fe and Ni, respectively.

3.2.3. *Silicon and Carbon*

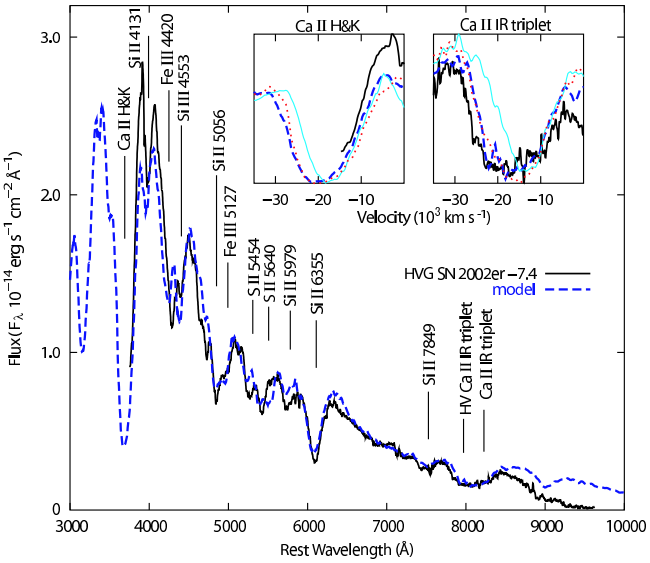

FIG. 4.— Observed spectrum of the HVG SN 2002er at day −7.4 (black solid) and a model with W7-CSM density/abundance structure (blue dashed). As in fig. 1, the left inset shows Ca II H&K, the right inset Ca II IR. The W7-CSM spectrum is compared to W7 (thin cyan) and DD (dotted red) models, both with homogeneous abundance and without CSM interaction.

The Si II λ5979 line is quite strong, which is consistent with the low photospheric temperature in the synthetic spectrum. The Si II λ6355 line in SN 2002dj is the broadest of the 6 SNe. In the model, the mass fraction of Si is X(Si)= 0.50 at the photosphere. The synthetic profile does not show enough absorption in the blue wing, as was the case for SN 2002bo, suggesting the presence of a Si II HVF. The emission profile of Si II λ6355 is well developed and there is no evidence of an absorption by C II λ6578.

3.2.4. *Calcium*

The Ca II HVF in SN 2002dj is the strongest of the 6 SNe. Even assuming X(Ca)=0.80 at the corresponding velocity range, the profile is not reproduced with the W7 density structure (the thin cyan line in insets of Fig. 3 is a homogeneous abundance model with X(Ca)=0.02). The blue dashed line is a synthetic spectrum obtained with a density jump at $v > 23,000$ km s^{-1} (adding 0.005 $M_\odot$), where X(H) = 0.30 and X(Ca) = 0.10. This hydrogen mass fraction is an upper limit for the absence of Hα again (M(H) $\sim 2\times10^{-3}M_\odot$). Using the DD density structure, the Ca mass fraction at high-velocity layers is reduced to X(Ca)=0.02 (assuming no CSM interaction, red dotted lines in the insets of Fig. 3) and X(Ca)=0.005 (assuming CSM interaction), respectively.

3.3. *SN 2002er (Day −7.4, HVG)*

3.3.1. *General Properties*

The spectra of the HVG SN 2002er were studied by Kotak et al. (2005). We use the earliest spectrum that covers the Ca II IR triplet (−7.4 days). A synthetic spectrum with log$L$ (erg s^{-1}) = 42.98 and $v_{\rm ph}$ = 9,500 km s^{-1} provides the best fit (Fig. 4). The lower $v_{\rm ph}$ agrees with the fact that this SN has lower line velocities than other HVG SNe (Kotak et al. 2005; B05). At the same time, $T_{\rm ph}$ = 17,300 K, higher than in both SNe 2002bo and 2002dj. This results from the combination of the higher L and lower $v_{\rm ph}$.

3.3.2. *Iron-group Elements*

Fe III lines contribute to the blue absorption near 4300Å (Fe III λ4396, 4420, 4431). At 4800Å, Fe III lines (e.g., λ5127) dominate over Fe II lines (e.g., λ5018), because the temperature is higher than in SNe 2002bo and 2002dj. To get sufficiently strong Fe lines, X(Fe)=0.013 near the photosphere. Although the lack of spectral coverage at $\lambda < 3800$Å makes it difficult to estimate the abundances of Ni and Co (see §3.1.2), an upper limit for these elements can be estimated as $X(^{56}{\rm Ni})_0$ <0.025 considering the absence of Ni II λ4067. Therefore, the mass fraction of stable Fe is $X({\rm Fe})_0$ =0.012-0.013.

3.3.3. *Silicon and Carbon*

Around 4300Å, Si III (λ4553, 4658) lines are stronger than in other HVG SNe, indicating a higher temperature. The blue wing of Si II λ6355 is also reproduced fairly well, and there is no clear evidence of a Si II HVF, unlike SNe 2002bo and 2002dj. C II λ6578 is not seen, but the Si II emission peak is weaker than in SNe 2002bo and 2002dj. A weak absorption near 7500Å is mostly due to Si II λ7849, and the contribution of Mg II λ7869 is small.

3.3.4. *Calcium*

The Ca II IR triplet is again not accounted for by the density structure of W7 (thin cyan lines in the insets of Fig. 4 show the profile of one-zone abundance model with X(Ca)=0.05). With the original W7 density structure, a Ca-dominated layer [X(Ca) $\sim$ 0.40] is required for the feature, which is highly unrealistic. The line depth and width can be reproduced with a density jump at $v > 21,000$ km s^{-1}, increasing the mass by 0.015 $M_\odot$ and containing X(H) = 0.30 (M(H)$\sim 5\times10^{-3}M_\odot$) and X(Ca) = 0.05, which is similar to SNe 2002bo and 2002dj. If the DD model density profile is used instead, the feature is reproduced with X(Ca)=0.05 at $v > 21,000$ km s^{-1} even without CSM interaction (insets of Fig. 4, dotted red lines). If CSM interaction is considered, this is further reduced to X(Ca)=0.007.

3.4. *SN 2001el (Day −9.0, LVG)*

3.4.1. *General Properties*

The LVG SN 2001el was studied in spectroscopy (Mattila et al. 2005) and spectropolarimetry (Wang et al. 2003). The best-fitting synthetic spectrum has log$L$ (erg s^{-1}) = 42.87 and $v_{\rm ph}$ = 10,500 km s^{-1} (Fig. 5). This leads to $T_{\rm ph}$ = 17,400 K, which is similar to SN 2002er, as can be expected since the spectra are similar.

3.4.2. *Iron-group Elements*

As in SN 2002er, the features around 4300 Å and 4800 Å are attributed mostly to Fe III lines. An iron mass fraction X(Fe) = 0.055 at the photosphere is needed to reproduce these features. Relatively reliable flux data at $\lambda \sim 3300-3500$ Å makes it possible to estimate the mass fractions of Ni and Co reliably (see 3.1.2): $X(^{56}{\rm Ni})_0$=0.19 provides the best fit. Thus the mass fraction of stable Fe is estimated as $X({\rm Fe})_0$=0.048.

3.4.3. *Silicon and Carbon*

The narrow Si III feature near 4400 Å has similar strength as in SN 2002er, supporting the similar photospheric velocity and temperature. The Si II λ6355 absorption has a boxy profile and is not reproduced well by the synthetic spectrum,

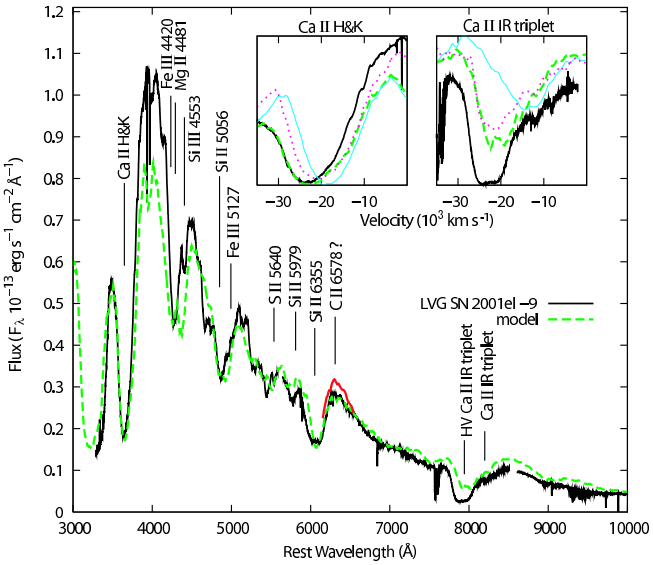

FIG. 5.— Observed spectrum of the LVG SN 2001el at day –9 (black solid) and a model with W7-CSM density/abundance structure (green dashed). The red solid line shows the profile without C in the ejecta. As in fig. 1, the left inset shows Ca II H&K, the right inset Ca II IR. The W7-CSM spectrum is compared to W7 (thin cyan) and DD (dotted red) models, both with homogeneous abundance and without CSM interaction.

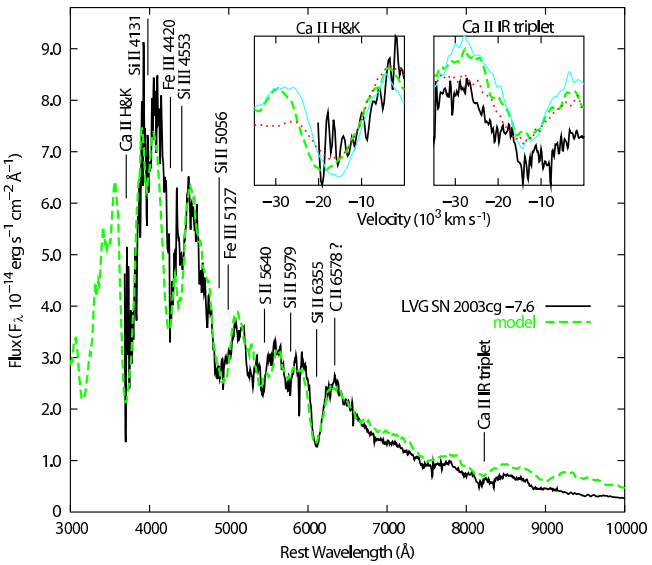

FIG. 6.— Observed spectrum of the LVG SN 2003cg at day –7.6 (black solid) and a model with W7-CSM density/abundance structure (green dashed). This model uses stratification with three abundance zones (§3.5.3). As in Fig. 1, the left inset shows Ca II H&K, the right inset Ca II IR. The W7-CSM spectrum is compared to W7 (thin cyan) and DD (dotted red) models, both with homogeneous abundance and without CSM interaction.

suggesting a contribution from HVFs. Similar profiles were also seen in SNe 1990N (Leibundgut et al. 1991; Mazzali 2001) and 2005cf (Garavini et al. 2007).

The Si II λ6355 emission peak is not as round and well developed in SN 2001el as in SNe 2002bo and 2002dj. The synthetic spectrum computed including C (Fig. 5, dashed green line) reproduces the feature well. If C is not included, the emission peak becomes too strong (Fig. 5, red line). This may be a sign of the presence of C. The C abundance required for the feature is, however, only $X(\mathrm{C}) \sim 0.005$. The mass of C is estimated as $\mathrm{M(C)} \sim 0.02 M_\odot$ assuming the W7 density structure and a homogeneous C mass fraction above the photosphere. Since C II λ6578 is the strongest optical C line, the presence of this amount of C does not affect other parts of the spectrum.

3.4.4. *Calcium*

As in other SNe, the Ca II HVFs cannot be reproduced with the W7 density structure (the thin cyan line in insets of Fig.5 shows the profile of a homogeneous abundance model with X(Ca)=0.02). The HVFs in SN 2001el are very strong and are not reproduced, even using X(Ca)=0.80 at high velocities. A better match is obtained using a density jump of a factor of 4 at $v \gtrsim 21,500$ km s^{-1}, adding a mass of 0.015 $M_\odot$, mixed-in hydrogen (X(H)=0.30, M(H)$\sim 5\times10^{-3} M_\odot$), and X(Ca)=0.10 (insets of Fig 5, dashed green line), but the synthetic Ca II IR triplet is too narrow. It may be made broader by increasing Ca mass fraction or using a larger density jump, but both changes seem unlikely and lead to a worse fit of Ca II H&K. A large Ca mass fraction, X(Ca)=0.10 in the high-velocity layers, is needed even with the DD density structure (insets of Fig. 5, dotted red lines). If CSM interaction is considered for the DD model, this is, however, reduced to X(Ca)=0.02.

3.5. *SN 2003cg (Day –7.6, LVG)*

3.5.1. *General Properties*

The LVG SN 2003cg was studied by Elias-Rosa et al. (2006). A synthetic spectrum with $\log L$ (erg s^{-1}) = 42.84 and $v_{\rm ph}$ = 9,000 km s^{-1} provides the best fit (Fig. 6). The model has $T_{\rm ph}$ = 17,000 K, similar to SNe 2002er and 2001el but higher than SNe 2002bo and 2002dj.

3.5.2. *Iron-group Elements*

To account for the strength of the Fe II and Fe III features at 4000-4900 Å, X(Fe)$\sim$ 0.036. We estimate an upper limit for ^{56}Ni of $X(^{56}\mathrm{Ni})_0 < 0.066$ from the absence of the Ni II λ4067 line. The mass fraction of stable Fe is therefore $X(\mathrm{Fe})_0 = 0.033 - 0.036$. A similar result is obtained in Elias-Rosa et al. (2006), but the mass fraction of stable Fe they find is only $X(\mathrm{Fe})_0$=0.015. The main difference is that $v_{\rm ph}$ is lower in our model, leading to a higher temperature and suppressing Fe II. In our model, the fraction of Fe II is smaller than in Elias-Rosa et al. (2006) by a factor of 3.

3.5.3. *Silicon and Carbon*

SN 2003cg has the narrowest Si II λ6355 line of our 6 SNe, although the line velocities are typical for LVG (Elias-Rosa et al. 2006). To reproduce the narrow feature, we use a layer at $v \sim 17,000 - 20,500$ km s^{-1} with a smaller Si mass fraction [X(Si) = 0.08] than at the photosphere [X(Si) = 0.40]. There is no evidence of a Si II HVF, which seems consistent with the weakness of the Ca II HVF (§3.5.4). The emission peak is somewhat suppressed, as in SNe 2002er and 2001el. Elias-Rosa et al. (2006) identified this as C II λ6578, who obtained a strong synthetic C II line useing X(C)=0.05. We find that 0.002 is an upper limit at the photosphere. However, C is not necessarily needed and the identification is not conclusive.

3.5.4. *Calcium*

While the Ca II IR HVF might be present in SN 2003cg, it is the weakest of the 6 SNe. In fact, a synthetic spectrum computed with the W7 density structure and homogeneous abundances [X(Ca)=0.02] (insets of Figure 6, thin

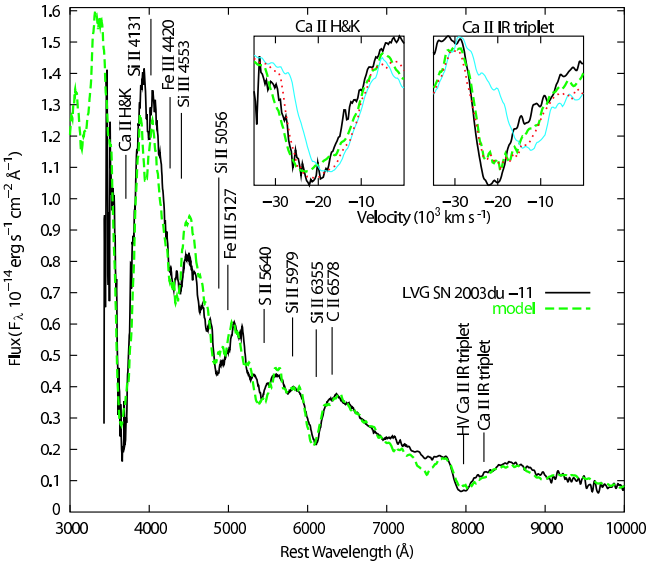

FIG. 7.— Observed spectrum of the LVG SN 2003du at day −11 (black solid) and a model with W7-CSM density/abundance structure (green dashed). As in Fig. 1, the left inset shows Ca II H&K, the right inset Ca II IR. The W7-CSM spectrum is compared to W7 (thin cyan) and DD (dotted red) models, both with homogeneous abundance and without CSM interaction.

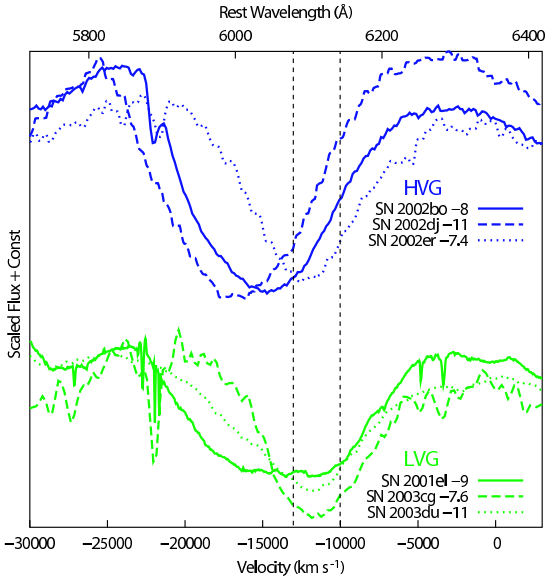

FIG. 8.— Observed Si II λ6355 features of 3 HVG SNe Ia (top, blue) and 3 LVG SNe Ia (bottom, green). Velocities and shapes of the blue wing differ among the objects. They range from 15,000 km s^{-1} to 25,000 km s^{-1} irrespective of the SN group (HVG, §4.1 or LVG, §4.2). The black dashed lines correspond to Doppler velocities of v = 10,000 and 13,000 km s^{-1}, which are the typical photospheric velocities of LVG and HVG, respectively.

cyan line) provides a reasonably good match to the observed profile, although a better match is obtained for a slightly higher Ca abundance [X(Ca)=0.03] at high velocity than at the photosphere [X(Ca)=0.02]. In the context of CSM interaction, i.e., a density jump by a factor of 4 and X(H)=0.30 (M(H)$\sim 5\times10^{-3}M_\odot$) at $v \gtrsim 21,000$ km s^{-1}, X(Ca)=0.001 is enough for the HVF. With the DD density structure a smaller fraction of Ca is required, as expected [X(Ca)=0.001 (0.0001) without (with) CSM interaction].

3.6. *SN 2003du (Day −11.0, LVG)*

3.6.1. *General Properties*

The LVG SN 2003du was studied by Stanishev et al. (2007). A synthetic spectrum with log$L$ (erg s^{-1}) = 42.71 and $v_{\rm ph}$ = 10,000 km s^{-1} gives the best agreement with the observed spectrum (Fig. 7). These parameters lead to $T_{\rm ph}$ = 18,600 K, which is close to that of other LVG SNe.

3.6.2. *Iron-group Elements*

The Fe III feature near 4300 Å is weaker than in SNe 2002el and 2003cg, but the temperature is not significantly different, suggesting a smaller Fe abundance at the photosphere: X(Fe) = 0.003 (determined as in §3.1.2) is enough to obtain this feature. We estimate the Ni mass fraction as $X(^{56}{\rm Ni})_0$=0.005 from the feature at 3900 Å. Thus, almost all the Fe contributing to the spectrum is likely to be stable.

3.6.3. *Silicon and Carbon*

The Si II λ6355 line is relatively weak and can be reproduced with a Si mass fraction of X(Si)=0.3. In spite of the low velocity of the absorption minimum, the blue wing of the absorption extends to $v\sim20,000$ km s^{-1}. Although this could be a sign of high-velocity material as in SNe 2002bo, 2002dj and 2001el, the line profile is different from other SNe, and the high-velocity absorption ($v\sim15,000-20,000$ km s^{-1}) is relatively weak (Mazzali et al. 2005b).

The emission peak of the line is suppressed, as seems common among LVG SNe. Including carbon with X(C) $\sim$ 0.003 improves the fit. If the identification is correct, the mass of C is estimated to be M(C)$\sim 0.001M_\odot$ assuming the W7 density structure and a homogeneous C mass fraction above the photosphere.

3.6.4. *Calcium*

The Ca II IR triplet at day −5 was studied by Gerardy et al. (2004). The spectrum at day −11 also shows a conspicuous HVF (Fig. 7), with profile and strength similar to those of SN 2001el. A very large high-velocity Ca mass fraction [X(Ca)>0.7] is required if W7 is used (thin cyan lines in the insets of Fig. 7 show the profile of a homogeneous abundance model with X(Ca)=0.016). For the CSM interaction scenario, we need X(Ca)=0.11 at high velocities ($v\gtrsim22,000$ km s^{-1}), where the density is increased by a factor of 4, adding 0.012 $M_\odot$, and X(H) is assumed to be 0.30 (M(H)$\sim 5\times10^{-3}M_\odot$, dashed green line in insets of Fig. 7). Even if the DD density structure is adopted, a high mass fraction of Ca at high velocity is required [X(Ca)=0.10]. This is reduced to X(Ca)=0.015 when CSM interaction is assumed(see Table 3).

4. DISCUSSION

We have modelled the pre-maximum spectra of 6 different SNe Ia (see Table 1). Three of these (2002bo, 2002dj and 2002er) are classified as High Velocity Gradient (HVG), and are characterized by a large Si line velocity that evolves rapidly after maximum brightness. The other three SNe (2001el, 2003cg, and 2003du), classified as Low Velocity Gradient (LVG), have a smaller Si line velocity that evolves slowly after maximum. The parameters of our models are shown in Tables 2 (luminosity and photospheric velocity) and 3 (abundances).

In the following, we summarize the properties of HVG (§4.1) and LVG (§4.2) SNe. Their different appearance stems

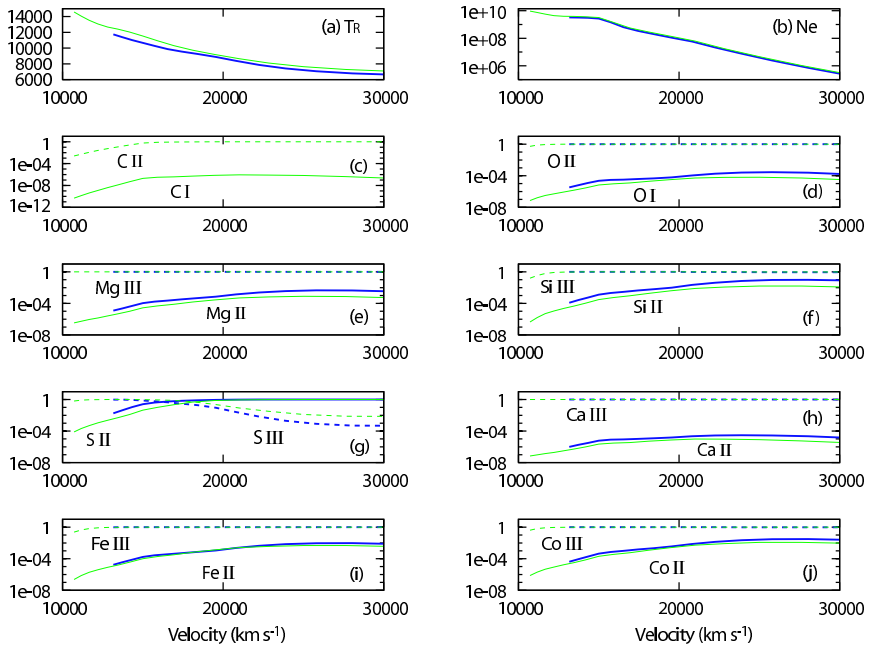

FIG. 9.— Radial distribution of (a) radiation temperature (K), (b) number density of electrons (cm^{-3}) and (c)-(j) ionization fraction of each element. Blue lines show the values for a HVG SN (2002bo) and green lines for a LVG SN (2001el). The two dominant ionization states are shown inside each panel; solid lines represent the lower state (e.g., C I, O I, Mg II). In panel (c), no blue lines appear, because C is not included in the models of HVG SNe.

basically from a different photospheric velocity. The presence of iron-peak elements in the outer layers is revisited and its implications are discussed in §4.3. Then, the origin of the difference between HVG and LVG is discussed in §4.4. The variety of High Velocity Features (HVFs) is very large independently of the classification of HVG or LVG. The causes for HVFs are also discussed in §4.5. Finally, possible influences to the LC width-luminosity relation are discussed (§4.6).

4.1. *The Properties of HVG SNe*

HVG SNe 2002bo and 2002dj have the highest line velocities and the lowest photospheric temperatures of the 6 SNe. The higher temperature for SN 2002er results from the high L and the low $v_{\rm ph}$. SN 2002er seems to be intrinsically more luminous than SN 2002bo at a similar epoch (Table 2), although it has a larger decline rate. This is also supported by the analysis of nebular spectra (Mazzali et al. 2007). The velocity of SN 2002er is intrinsically lower than that of other HVG SNe (B05; Kotak et al. 2005). Although a SN may be classified as HVG, its T_{eff} can be as high as that of LVG SNe if the SN has both a high enough L and low enough $v_{\rm ph}$. This suggests continuity between two groups (Branch et al. 2006, 2007).

The Si II λ6355 lines of SNe 2002bo and 2002dj have well-defined P-Cygni profiles with blue wings reaching $v \sim 23,000$ km s^{-1} (blue lines in Fig. 8). In the spectra of these SNe, C II is not seen below at least $v = 20,000$ km s^{-1}. This suggests that the abundance distribution of HVG SNe resembles that of 1D delayed detonation models (Khokhlov et al. 1991a; Höflich & Khokhlov 1996; Iwamoto et al. 1999) rather than that of the 1D deflagration model W7 (Nomoto et al. 1984).

The computed physical conditions in the ejecta of a representative HVG SN, 2002bo, and those of a typical LVG SN of similar Δm_{15}, and thus presumably similar luminosity, SN 2001el, are shown in Figure 9. In the ionization plot, solid lines represent the lower of two states marked in each panel. The temperature structure, the number density of electrons, and the ionization state of SN 2002bo and SN 2001el computed under the assumptions described in §2 are rather similar at all layers with $v > 12,900$ km s^{-1}. Consequently, the ionization fractions are also similar.

B05 show the evolution of the parameter $\mathcal{R}$(Si), the ratio of the Si II lines at 5800 and 6000 Å. $\mathcal{R}$(Si) is thought to be a temperature indicator (Nugent et al. 1995). At pre-maximum epochs ($\lesssim -10$ days), $\mathcal{R}$(Si) is larger in HVG than in LVG SNe (see Fig. 2 in B05). As we have shown, a typical HVG SN has a lower photospheric temperature before maximum. The fact that SNe 2002bo and 2001el have a similar Δm_{15}, and therefore should have a similar luminosity, suggests that the lower temperature of SN 2002bo at pre-maximum epochs reflects its higher photospheric velocity. Therefore, $\mathcal{R}$(Si) is not a good indicator of SN luminosity at pre-maximum phases, when the dispersion of the photospheric velocity among different SNe is still very large (B05). On the other hand, since the diversity in photospheric velocity is small at epochs near maximum, both $\mathcal{R}$(Si) and the temperature more closely reflects the intrinsic luminosity.

4.2. *The Properties of LVG SNe*

The three LVG SNe have similar photospheric velocities and temperatures. The temperature structure, electron density, and ionization state of SN 2001el are shown in Figure 9 (green lines). The run of all physical quantities is similar to HVG SN 2002bo at comparable velocities, but the values at the photosphere are significantly different because $v_{\rm ph}$ is lower for LVG. In particular, important ions such as Si II, S II, Ca II, and Fe II are a factor of > 10 less abundant near the photosphere of LVG SNe (at $v \sim 10,000$ km s^{-1}) then near the photosphere of HVG SNe (at $v \sim 13,000$ km s^{-1}).

The C II λ6578 line is likely to be present in the LVG SNe 2001el and 2003du, and possibly also in SN 2003cg near the photosphere ($v \sim 10,000$ km s^{-1}). The mass fraction of C required to suppress the Si II λ6355 emission peak is however only 0.002-0.003. The mass of C in SNe 2001el and 2003du

is only $\sim 0.001 M_\odot$ if we assume a homogeneous, spherically symmetric distribution above the photosphere. Even if we consider that we cannot estimate the C abundance at $v \gtrsim 18,000$ km s^{-1} because of the blend with the Si II line, and assume X(C)=0.5 at $v > 18,000$ km s^{-1}, the mass of C is at most $\sim 0.01 M_\odot$. This is still less than predicted by the W7 model ($\sim 0.05 M_\odot$).

Although C I is used to estimate C abundance in Marion et al. (2006), C I is not the dominant ionization state as shown in Figure 9 (solid line), and the exact amount of C I is very sensitive to the temperature structure. In our calculations, C I lines never become visible even if C II makes a deep absorption, suggesting that C II is a better indicator of carbon abundance in this temperature range.

Alternatively, the emission peak of Si II λ6355 may be suppressed if Si is detached from the photosphere (see Branch et al. 2002 for the case of Hα). This is however not the case for the objects presented here because the velocity of Si II decreases to $v < 9,000$ km s^{-1} at subsequent epochs and Si is abundant at the corresponding velocities. In addition to this, the fact that the emission profile of the Si II line is well-peaked at maximum light even in LVG suggests that the suppression is related to the conditions of the outer layers.

4.3. *Fe-group elements in the outer ejecta*

Both Fe II and Fe III lines are clearly present in pre-maximum spectra. We showed that about a few percent of Fe in mass fraction, including both stable Fe and decay products of ^{56}Ni, are required to match the observed lines (§3.1.2). Lines of both ions (Fe II and Fe III) are correctly reproduced, which suggests that the computation of the ionization state of Fe is reliable. The fact that Fe is not highly abundant indicates that the photosphere resides outside the Fe-rich layers.

In order to distinguish stable Fe (e.g., ^{54}Fe) from the decay product of ^{56}Ni (i.e., ^{56}Fe), the abundances of Ni and Co were quantified from the spectra (§3.1.2). In 4 of our SNe, we are able to estimate the ^{56}Ni abundance near the photosphere, while only upper limits could be obtained in the remaining 2 cases. If ^{56}Ni accounted for all the present Fe abundance at such an early epoch (when only 3% of ^{56}Ni has decayed to ^{56}Fe), the ejecta would be dominated by ^{56}Ni. This is, however, clearly inconsistent with the observed spectra and the parameters obtained from the modeling. Therefore, we conclude that not only ^{56}Ni, but also stable Fe must exist at the photosphere. The respective abundances obtained are always larger than solar suggesting that the origin is not the progenitor but nucleosynthesis during the explosion.

The metal abundances in the outer layers suggest that the abundances are not sharply stratified with velocity. Even in 1D, the region where ^{56}Ni is synthesized extends to Si-rich layers because the temperature changes smoothly during the explosion. ^{54}Fe can also be synthesized in Si-rich layers (e.g., Iwamoto et al. 1999). Another explanation for Fe-group elements in outer layers may be large scale mixing, as seen in recent three-dimensional deflagration models (e.g., Gamezo et al. 2003; Röpke & Hillebrandt 2005; Röpke et al. 2006).

The presence of Fe-group elements in the outer layers and the diversity of their abundances and a low abundance of unburned elements may hinder the use of pre-maximum spectra as indicators of the progenitor metallicity (Lentz et al. 2000). In fact, larger diversity than predicted by model computations is seen in UV spectra (Ellis et al. 2007). This may reflect diversity in the abundances of Fe-group elements in the outer layers, or in the photospheric temperature (§4.1 and 4.2).

4.4. *The Origin of the Difference between HVG and LVG SNe*

The difference between HVG and LVG SNe can be studied comparing the properties of SNe with similar decline rates (Δm_{15}). For an optimal comparison at a similar epoch, we again take SNe 2002bo (HVG; −8.0 days, Δm_{15} = 1.17) and 2001el (LVG; −9 days, Δm_{15} = 1.15) as examples.

The marginal detection of carbon in the emission peak of Si II λ6355 in LVG SNe suggests that the burning is less powerful in LVG SNe than in HVG SNe. It is also interesting that other SNe where C was detected (SN 1998aq, Branch et al. 2003; and possibly SN 1994D, Branch et al. 2005) are also LVG [15]. In addition, we find that HVG SNe do not have carbon at least up to $v \sim 20,000$ km s^{-1}.

If more burning occurs in HVG than in LVG SNe, the former may have more kinetic energy. This would tend to make the photospheric velocity of HVG higher. The kinetic energy difference between HVG and LVG can estimated by a simple analysis. We assume that the outermost layer are fully burned to Si in HVG while half of the material at $v > 18,000$ km s^{-1} is oxygen and carbon in LVG. Since the mass above v = 18,000 km s^{-1} is $\sim 0.02 M_\odot$ assuming the W7 density structure, the difference in nuclear energy release is $\sim 0.02 \times 10^{51}$ erg, which is less than $\sim 2\%$ of the typical kinetic energy of SNe Ia models. The expected difference in photospheric velocity is however only $\lesssim 1\%$. Therefore, it seems unlikely that the difference between HVG and LVG can be accounted for by a different kinetic energy alone. Yet, such a difference in kinetic energy cannot be ruled out.

Alternatively, HVG SNe may have more massive ejecta than LVG SNe. The limiting mass of a spinning WD can exceed the Chandrasekhar mass of the static WD, $\sim 1.38 M_\odot$ (Uenishi, Nomoto & Hachisu 2003; Yoon & Langer 2004, 2005; Domínguez et al. 2006). Since the density structure of a rotating WD is flatter than that of a static one, the photospheric velocity may be larger before maximum but then evolve more rapidly. Unless the WD mass is extremely large – such as the $2 M_\odot$ suggested for SN 2003fg by Howell et al. (2006), the expansion kinetic energy would not be significantly reduced by a higher binding energy. However, there is no evidence that HVG SNe tend to synthesize more ^{56}Ni, which does not support this interpretation.

Even though the mass and the kinetic energy of the ejecta are similar in HVG and LVG, a different Fe-group abundance in the outer region could make their appearance different. Some amount of Fe-group elements is present in the outer layers of all 6 SNe (see §4.3). Line velocities are expected to be higher if more Fe-group elements are present in the outer layers because of the larger opacity of these elements.

Our results show that the near-photospheric abundance of Fe-group elements is not smaller in HVG than in LVG, even though the photospheric velocity is higher in HVG by $\sim 2-3,000$ km s^{-1}. This might imply that HVG SNe have more Fe-group elements if the metal abundance is a decreasing function of radius (velocity). Therefore, the abundances of Fe-group elements in the outer layers can be a cause of spectral diversity, while differences in the kinetic energy or the progenitor mass are less likely. To confirm this hypothesis, the metal abundance in the spectra of LVG with $v_{\rm ph} \gtrsim 13,000$

[15] Since the number of LVG seems to be larger than that of HVG (B05; Mazzali et al. 2007), this could be a statistical effect.

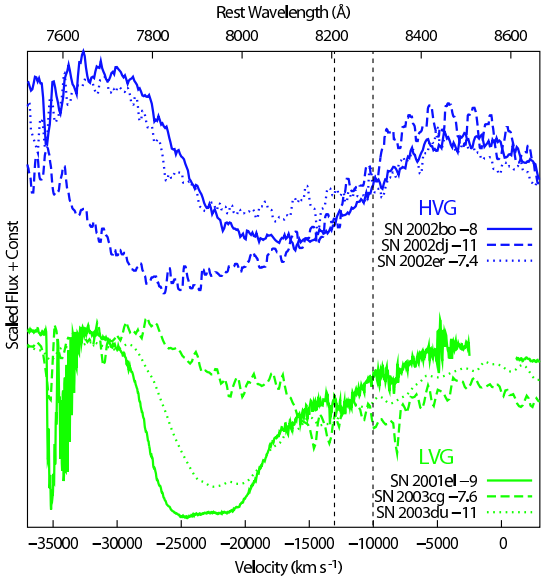

FIG. 10.— Ca II IR triplet profiles (a mean wavelength of 8567 Å is assumed) of 3 HVG SNe Ia (top, blue) and 3 LVG SNe Ia (bottom, green). In LVG SNe (SNe 2001el and 2003du in our sample and SN 2003kf in Mazzali et al. 2005b), HVFs tend to be detached, which is likely the consequence of the high photospheric temperature and the low photospheric velocity (see §4.5). On the other hand, the strength of the high-velocity absorption seems to be random (Tanaka et al. 2006). The dashed black, vertical lines correspond to Doppler velocities of $v = 10,000$ and $13,000$ km s^{-1}, which are the typical photospheric velocities of LVG and HVG, respectively.

km s^{-1} should be investigated with earlier spectra.

4.5. *High-Velocity Features*

High-velocity features ($v \gtrsim 20,000$ km s^{-1}) are seen in both Ca II H&K and in the IR triplet. Except for SN 2003cg, HVFs are not present in synthetic spectra based on W7. They can be reproduced using the DD density structure and a relatively large Ca abundance. Alternatively, they can be also explained by an enhancement in density of the outer layer ($v > 20-22,000$ km s^{-1}) of a factor of 4 from the W7 value assuming some H ($\sim 30\%$ in mass fraction) in this region. Interaction with CSM may produce the latter situation; mixing of H into the ejecta increases the Ca II fraction by a factor of 5-10 as it favors recombination (Mazzali et al. 2005a).

The profiles of the Ca II IR triplet show variations (Fig. 10). In HVG SNe (blue lines), the profile is round and the high-velocity component tends to blend with the photospheric component. In LVG SNe, on the other hand, the profiles are less blended because of the weakness of the photospheric component (green lines, see also SN 2003kf in Mazzali et al. 2005b). This is a natural consequence of the high $T_{\rm ph}$ and the low $v_{\rm ph}$ of LVG SNe. The high temperature suppresses Ca II and Si II lines near the photosphere, and the low photospheric velocity makes the position of the photospheric component redder. The combination of these two effects results in a weaker and redder photospheric absorption, so that the high-velocity component becomes more detached in LVG SNe.

The strength of the high-velocity component also varies from SN to SN. As our models show, this is not a temperature effect, because the temperature in the outer region is similar in all cases (Fig. 9). Although we could reproduce the strength of the HVF increasing the Ca abundance, the abundances that are required show a large spread (of a factor of 100; Table 3). This diversity may be a line-of-sight effect if HVFs are caused by aspherical structures, like a torus or clumps (Tanaka et al. 2006), as also suggested by the high polarization level of the feature (Wang et al. 2003; Kasen et al. 2003).

The very strong, broad blue wing of the Si II λ6355 absorption in SNe 2002bo, 2002dj and 2001el is not perfectly explained by our synthetic spectra (Figures 1, 3 and 5). This suggests the presence of HVFs in Si II as well as in Ca II lines, although the velocity of the blue edge of the Si II absorption is lower than that of the Ca II lines (Figures 8 and 10). On the other hand, SNe 2002er, 2003cg and 2003du lack this feature (Figures 4, 6, and 7).

The origin of HVFs is debated (e.g., Hatano et al. 1999; Wang et al. 2003; Thomas et al. 2004; Gerardy et al. 2004; Mazzali 2005a; Kasen & Plewa 2005; Tanaka et al. 2006). The difficulty in using the DD model is that it still requires a high Ca abundance in the high-velocity layers ($v \gtrsim 23,000$ km s^{-1}; Table 3) despite the absence of a very strong Si absorption at similar velocities. One problem with the CSM interaction scenario is that it requires the accumulation of a relatively large mass. The estimated mass in the high-velocity shell is $\sim 0.01 M_\odot$. In order to accumulate this mass, a mass loss rate $\dot{M} \sim 10^{-4}\ M_\odot$ yr^{-1} is required for a wind velocity of 10 km s^{-1}. This mass loss rate is higher than that constrained from X-ray, optical and radio observations (e.g., Cumming et al. 1996; Mattila et al. 2005; Immler et al. 2006; Hughes et al. 2007; Panagia et al. 2006). A combination of these two scenarios (i.e., DD model and CSM interaction) may relax these requirements (Gerardy et al. 2004).

Alternatively, HVFs may reflect the pre-SN abundances of the progenitor WD. In the single-degenerate scenario, the WD accretes matter from a companion star (see Nomoto et al. 1994 for a review). At an accretion rate suitable for stable H shell burning (Nomoto 1982), He shell flashes are rather weak (Taam 1980; Fujimoto & Sugimoto 1982), and their products can accrete onto the WD.

The products of He shell flashes could be Ca-rich depending on conditions such as the pressure at the burning shell (Hashimoto, Hanawa & Sugimoto 1983). After many cycles of He flashes, when the mass of the WD reaches the Chandrasekhar mass, the outermost layers of the WD should consist not only of C and O but also of heavier elements. If such matter resides in the outermost layers after the explosion, it could cause HVFs. To investigate this scenario further, the growth of the WD should be studied in detail.

If Si II and Ca II HVFs are caused by the explosion itself or by CSM interaction, they should correlate (see Fig. 12 in Tanaka et al. 2006). In fact, this seems to be the case for SNe 2002bo, 2002dj, 2001el, and 2003cg, but the correlation is not clear for SNe 2002er and 2003du [16] (Figs. 8 and 10). This may be useful to discriminate the origin of the HVFs.

4.6. *Implications for the Width-Luminosity Relation*

The relation between LC width and luminosity in SNe Ia indicates that the properties of SNe Ia are determined by a single dominant parameter. However, dispersion is present in the relation, and it may due to uncertainties in distance and reddening or to intrinsic properties of SNe Ia (Mazzali & Podsiadlowski 2006). Understanding the origins of the dispersion is important for a more precise cosmological use of SNe Ia.

The earliest spectra of SNe Ia are clearly not determined by a single parameter, e.g., SNe with a similar maximum lu-

[16] Si and Ca HVF may correlate in an earlier spectrum of SN 2003du. See Stanishev et al. (2007).

minosity have different line velocities. Therefore, the variation in the early phase spectra could, to some extent, reveal an intrinsic dispersion in the width-luminosity relation. Since the variation of properties is larger in HVG than in LVG SNe (B05; Mazzali et al. 2007), the HVG group at least could be related to the dispersion in the width-luminosity relation.

A first parameter to look at in this context is the kinetic energy of the ejecta. HVG SNe may have higher kinetic energy than LVG by at most $\sim 2\%$ (§4.4). Since the light curve width ($\tau_{\rm LC}$) scales roughly as $\tau_{\rm LC} \propto E_{\rm K}^{-1/4}$ (Arnett 1982), where $E_{\rm K}$ is the kinetic energy of the ejecta, the LC width of HVG SNe may become narrower than that of LVG SNe. This effect should not be significant given the dependence of $\tau_{\rm LC}$. However, an earlier LC rise, accompanied by a brighter luminosity at maximum even when the ejecta contain the same amount of ^{56}Ni, is a change orthogonal to the observed width-luminsity relation. Thus, differences in $E_{\rm K}$ could cause an intrinsic dispersion in the width-luminosity relation.

The ^{56}Ni distribution could also affect the LC rise time. If HVG SNe have an extended ^{56}Ni distribution as suggested in §4.4, their LC may peak earlier than in the case where ^{56}Ni is confined in the innermost layers because the diffusion time is shorter for the outer ^{56}Ni. An early LC rise would make the peak luminosity brighter even for the same ^{56}Ni mass. Consequently, SNe with similar Δm_{15} may have different peak luminosities in certain conditions of mixing (e.g., Mazzali & Podsiadlowski 2006, Woosley et al. 2007).

5. CONCLUSIONS

The outermost ejecta of Type Ia SNe are studied by modeling very early spectra. Of the 6 SNe we studied, 2 (SNe 2002bo and 2002dj) are classified as HVG, being characterized by a high photospheric velocity and a low photospheric temperature. All three LVG SNe (SNe 2001el, 2003cg and 2003du) have uniform properties and are characterized by a low photospheric velocity and a high photospheric temperature. The properties of SN 2002er, which is classified as HVG, are close to those of LVG, suggesting that there is continuity between the groups. This is consistent with suggestions by Branch et al. (2006, 2007)

HVG SNe have a Si II λ6355 line with a pronounced emission peak and a broad blue absorption, suggesting that Si is present at $v > 20,000$ km s^{-1}. The abundance distribution in HVG SNe is similar to that of a delayed detonation model, i.e., the burning front reaches the outermost layers. On the other hand, the Si II λ6355 emission profile of LVG SNe tends to be suppressed, possibly because of the presence of C II λ6578. This suggests that the burning front in LVG SNe is weaker than in HVG SNe. However, the mass fraction of carbon at the photosphere of LVG SNe is only $X({\rm C}) \lesssim 0.01$, and the estimated C mass is less than $\sim 0.01 M_\odot$, which is less than predicted by W7 ($\sim 0.05 M_\odot$).

The difference in the photospheric velocity explains the different appearance of HVG and LVG SNe at pre-maximum phases through the temperature difference. At the highest velocities ($v \gtrsim 20,000$ km s^{-1}), however, the variety of the Ca II and Si II features is not explained by this scenario. This may require additional factors such as asphericity or diversity in the element abundance of the progenitor WD.

Both stable Fe and ^{56}Ni are detected at the photosphere ($v = 9-14,000$ km s^{-1}) in all 6 SNe, suggesting that Fe-group elements are always present in the outer layers. The differece in their abundances may be an important reason for the diversity among SN Ia spectra. On the other hand, the difference in kinetic energy between HVG and LVG SNe is too small to be the origin of the spectral diversity.

The diversity of SNe Ia seen in early phase spectra could cause the intrinsic dispersion in the LC width-luminosity relation, through the difference in kinetic energy and the amount of iron-group elements in the outer layers.

M.T. is supported by the JSPS (Japan Society for the Promotion of Science) Research Fellowship for Young Scientists. G.P. acknowledges support by the Proyecto FONDECYT 3070034. This research was supported in part by the Grant-in-Aid for Scientific Research (18104003, 18540231) and the 21st Century COE Program (QUEST) from the JSPS and MEXT of Japan.

REFERENCES

Abbott, D.C., & Lucy, L.B. 1985, ApJ, 288, 679
Arnett, W.D. 1982, ApJ, 253, 785
Astier, P., et al. 2006, A&A, 447, 31
Baron, E., Bongard, S., Branch, D., Hauschildt, P. H. 2006, ApJ, 645, 480
Benetti, S., et al. 2004, MNRAS, 348, 261
Benetti, S., et al. 2005, ApJ, 623, 1011 (B05)
Bongard, S., Baron, E., Smadja, G., Branch, D., & Hauschildt, P.H. 2006, ApJ, 647, 513
Branch, D., et al. 2002, ApJ, 566, 1005
Branch, D., et al. 2003, AJ, 126, 1489
Branch, D., Baron, E., Hall, N., Melakayil, M., & Parrent, J. 2005, PASP, 117, 545
Branch, D., et al. 2006, PASP, 118, 560
Branch, D., et al. 2007, PASP, 119, 709
Cumming, R. J., Lundqvist, P., Smith, L. J., Pettini, M., King, D. L. 1996, MNRAS, 283, 1335
Domínguez, I., Piersanti, L., Bravo, E., Tornambe, A., Straniero, O., & Gagliardi, S. 2006, ApJ, 644, 21
Elias-Rosa, N., et al. 2006, MNRAS, 369, 1880
Ellis, R.S., et al. 2007, ApJ, in press (arXiv:0710.3896)
Fisher A., Branch D., Nugent P., Baron E., 1997, ApJ, 481, L89
Fujimoto, M. Y., & Sugimoto, D. 1982, 257, 291
Gamezo, V.N., Khokhlov, A., Oran, E.S., Chtchelkanova, A.Y. & Rosenberg, R.O. 2003, Science, 299, 77
Gamezo, V.N., Khokhlov, A., & Oran, E.S., 2005, ApJ, 623, 337
Garavini, G., et al. 2005, AJ, 130, 2278
Garavini, G., et al. 2007, A&A, 471, 527
Gerardy, C. L., et al. 2004, ApJ, 607, 391
Hatano, K., Branch, D., Fisher, A., Baron, E. & Filippenko, A.V. 1999, ApJ, 525, 881
Hatano, K., Branch, D., Lentz, E.J., Baron, E., Filippenko, A.V. & Garnavich, P.M. 2000, ApJ, 543, L49
Hachinger, S., Mazzali, P.A., & Benetti, S. 2006, MNRAS, 370, 299
Hashimoto, M.-A., Hanawa, T., & Sugimoto, D. 1983, PASJ, 35, 1
Hicken, M., Garnavich, P.M., Prieto, J.L., Blondin, S., DePoy, D.L., Kirshner, R.P., & Parrent, J. 2007, ApJ, 669, L17
Höflich P., & Khokhlov, A. 1996, ApJ, 457, 500
Howell, D.A., et al. 2006, Nature, 443, 308
Hughes, J. P., Chugai, N., Chevalier, R., Lundqvist, P., & Schlegel, E. 2007, ApJ, in press (arXiv:0710.3190)
Immler, S., et al. 2006, ApJ, 648, L119
Iwamoto, K., Brachwitz, F., Nomoto, K., Kishimoto, N., Umeda, H., Hix, W.P., & Thielemann, F-K. 1999, ApJS, 125, 439
Kasen, D., et al. 2003, ApJ, 593, 788
Kasen, D., & Plewa, T. 2005, ApJ, 622, L41
Khokhlov, A.M. 1991a, A&A, 245, L25
Khokhlov, A.M. 1991b, A&A, 245, 114
Klein, R. I., & Castor, J. I. 1978, ApJ, 220, 902
Knop, R.A., et al. 2003, ApJ, 598, 102
Kotak, R., et al. 2005, A& A, 436, 1021
Leibundgut, B., Kirshner, R. P., Filippenko, A. V., Shields, J. C., Foltz, C. B., Phillips, M. M., & Sonneborn, G. 1991, ApJ, 371, L23
Lentz, J.E., Baron, E., Branch, D., Hauschildt, P.H., & Nugent, P. 2000, ApJ, 530, 966
Lucy, L.B. 1999, A&A, 345, 211
Marion, G.H., Höflich, P., Wheeler, J.C., Robinson, E.L., Gerardy, C.L., & Vacca, W.D. 2006, ApJ, 645, 1392

Mattila, S., Lundqvist, P., Sollerman, J., Kozma, C., Baron, E., Fransson, C., Leibundgut, B., & Nomoto, K. 2005, A&A, 443, 649
Mazzali, P.A. & Lucy, L.B. 1993, A&A, 279, 447
Mazzali, P.A., Lucy, L.B., Danziger, I.J., Gouiffes, C., Cappellaro, E., & Turatto, M. 1993, A&A, 269, 423
Mazzali, P. A., Cappellaro, E., Danziger, I. J., Turatto, M., & Benetti, S. 1998, ApJ, 499, L49
Mazzali, P.A. 2000, A&A, 363, 705
Mazzali, P.A. 2001, MNRAS, 321, 341
Mazzali, P.A., Benetti, S., Stehle, M., Branch, D., Deng, J., Maeda, K., Nomoto, K. & Hamuy, M. 2005a, MNRAS, 357, 200
Mazzali, P.A., et al. 2005b, ApJ, 623, L37
Mazzali, P.A., & Podsiadlowski, P. 2006, MNRAS, 369, L19
Mazzali, P.A., Röpke, F.K., Benetti, S., & Hillebrandt, W. 2007, Science, 315, 825
Nomoto, K., Sugimoto, D., & Neo, S. 1976, Ap&SS, 39, L37
Nomoto, K. 1982, ApJ, 253, 798
Nomoto, K., Thielemann, F.-K., & Yokoi, K. 1984, ApJ, 286, 644
Nomoto, K., Yamaoka, H., Shigeyama, T., Kumagai, S., & Tsujimoto, T. 1994, Bludman S. A., Mochkovitch R., Zinn-Justin, eds., Les Houches Session LIV, Supernovae, Elsevier, Amsterdam, 199
Nugent, P., Phillips, M., Baron, E., Branch, D., & Hauschildt, P. 1995, ApJ, 455, L147
Panagia, N., Van Dyk, S. D., Weiler, K. W., Sramek, R. A., Stockdale, C. J., & Murata, K. P. 2006, ApJ, 646, 369
Perlmutter, S., et al. 1999, ApJ, 517, 565
Phillips, M.M. 1993, ApJ, 413, L105
Phillips, M.M., Lira, P., Suntzeff, N. B., Schommer, R. A., Hamuy, M., & Maza, J. 1999, AJ, 118, 2688
Pignata, G., et al. 2004, MNRAS, 355, 178
Pignata, G., et al. 2005, ASP Conf. Ser. 342, 1604-2004: Supernovae as Cosmological Lighthouses, ed. M. Turatto, S. Benetti, L. Zampieri, & W. Shea (San Francisco: ASP), 266
Pinto, P.A., & Eastman, R.G. 2000, ApJ, 530, 757
Plewa, T., Calder, A.C., & Lamb, D. Q. 2004, ApJ, 612, L37
Quimby, R., Höflich, P., Kannappan S.J., Rykoff E., Rujopakarn W., Akerlof C.W., Gerardy C.L., & Wheeler J.C. 2006, ApJ, 636, 400
Reinecke, M., Hillebrandt, W. & Niemeyer, J. C. 2002, A& A, 391, 1167
Riess, A. G., et al. 1998, AJ, 116, 1009
Riess, A. G., et al. 2004, ApJ, 607, 665
Röpke, F., K. & Hillebrandt, W. 2005, A& A, 431, 635
Röpke, F. K., Gieseler, M., Reinecke, M., Travaglio, C., & Hillebrandt, W. 2006, A&A, 453, 203
Stanishev, V. et al. 2007, A& A, 469, 645
Stehle, M., Mazzali, P.A., Benetti, S., & Hillebrandt, W. 2005, MNRAS, 360, 1231
Taam, R. E. 1980, ApJ, 237, 142
Tanaka, M., Mazzali, P.A., Maeda, K., & Nomoto, K. 2006, ApJ, 645, 470
Thomas, R. C., Branch, D., Baron, E., Nomoto, K., Li, W., Filippenko, A. V. 2004, ApJ, 601, 1019
Thomas, R. C, et al. 2007, ApJ, 654, L53
Travaglio, C., Hillebrandt, W., Reinecke, M., & Thielemann, F.-K. 2004, A& A, 425, 1029
Uenishi, T., Nomoto, K., & Hachisu, I. 2003, ApJ, 595, 1094
Wang, L., et al., 2003, ApJ, 591, 1110
Wood-Vasey, W.M., et al. 2007, ApJ, 666, 694
Woosley, S. E., Kasen, D., Blinnikov, S., & Sorokina, E. 2007, ApJ, 662, 487
Yoon, S.C., & Langer, N. 2004, A&A, 419, 623
Yoon, S.C., & Langer, N. 2005, A&A, 435, 967